

General Treatment of Reflection of Spherical Electromagnetic Waves from a Spherical Surface and its Implications for the ANITA Anomalous Polarity Events

Paramita Dasgupta* and Pankaj Jain†

Department of Physics,

Indian Institute of Technology, Kanpur

Kanpur, India- 208016

(Dated: April 10, 2019)

Abstract

We develop a general formalism to treat reflection of spherical electromagnetic waves from a spherical surface. Our main objective is interpretation of radio wave signals produced by cosmic ray interactions with Earth's atmosphere which are observed by the Antarctica based ANITA detector after reflection off the ice surface. The incident wave is decomposed into plane waves and each plane wave is reflected off the surface using the standard Fresnel formalism. For each plane wave the reflected wave is assumed to be locally a plane wave. This is a very reasonable assumption and there are no uncontrolled approximations in our treatment of the reflection phenomenon. The surface roughness effects are also included by using a simple model. We apply our formalism to the radiation produced by the balloon-borne HiCal radio-frequency (RF) transmitter. Our final results for the reflected power are found to be in good agreement with data for all elevation angles. We also study the properties of reflected radio pulses in order to study their phase relationship with direct pulses. We find that for some roughness models the pulse shape can be somewhat distorted and may be misidentified as a direct pulse. However this is a rather small effect and is unable to provide an explanation for the observed mystery events by ANITA.

* paromita@iitk.ac.in

† pkjain@iitk.ac.in

I. INTRODUCTION

The NASA sponsored balloon-borne ANITA detector [1–4] operating in Antarctica is designed to detect ultra high energy cosmic rays (UHECR) with energies exceeding 1 EeV (10^{18} eV) [5] by collecting the radio pulse generated through the interaction of the primary particle with Earth’s atmosphere [6–8]. The radio pulse is detected after reflection from the Antarctic ice surface. For calibration and measurement of surface reflectivity, the balloon-borne HiCal radio-frequency (RF) transmitter is used. In a recent paper [9] we developed a theoretical formalism to analyse the process of reflection of such pulses from the ice surface. The pulse can be considered as a superposition of spherical waves with a chosen spectral profile. Here we are interested in determining the mean value of reflection coefficient over the range of frequencies which are of interest in HiCal observations. Previously, the surface reflectivity was deduced from ANITA-2 [10] and ANITA-3 observations of the Sun, and also ANITA-3 measurements of HiCal-1 pulses [11]. More details on the instrument can be found in [12, 13] and [14]. The formalism we use in this paper is based on decomposition of a spherical wave in terms of plane waves [15]. This can be represented as

$$\frac{e^{ikr}}{r} = \frac{ik}{2\pi} \int_0^{2\pi} \int_0^{\frac{\pi}{2}-i\infty} e^{ik[x \sin \alpha \cos \beta + y \sin \alpha \sin \beta + (z_0 - z) \cos \alpha]} \sin \alpha d\alpha d\beta \quad (1)$$

where α, β are the spherical polar coordinates and this decomposition is valid in the range $0 \leq z \leq z_0$. The reflection properties of each plane wave can be determined by imposing standard boundary conditions which lead to the Fresnel coefficients. The contributions over all such plane waves is added in order to determine the reflected wave at a given frequency. In [9] it was assumed that the reflected wave corresponding to each plane wave is also a plane wave. This assumption is not valid for a curved surface. By comparing our results with the HiCal data it was found to be in good agreement with observations for elevation angles greater than 10 degrees. The elevation angle is defined as the angle relative to the tangent at the surface at the point of specular reflection. The reason for this agreement is that the dominant contribution to the reflected wave is obtained from angles α, β close to the point of specular reflection. Over such small angles the deviation of reflected wave from a plane wave may not be very significant. However for small elevation angles it deviates considerably from observations. Here we develop a more reliable procedure which only assumes that the reflected wave can be considered locally as a plane wave. This is a very

reasonable assumption since at any point we can define a tangent plane to the wave front which provides a good approximation to the wave front in a small neighbourhood of that point.

II. REFLECTION AND TRANSMISSION ON A FLAT SURFACE

We start by reviewing the formalism for the case of a flat surface since the resulting formulas would be used in the case of spherical surface. The basic geometry for this case is shown in Fig. 1. Here the source S lies at $(0, 0, z_0)$. Let \vec{E}_q denote the electric field vector for a particular incident plane wave. The subscript $q = i, r, t$ designates the incident, reflected and transmitted waves respectively. The corresponding magnetic field is denoted by \vec{H}_q . Here we are primarily interested in the H-pol which corresponds to the component of the electric field perpendicular to the plane of incidence. The complete Hertz potential for the direct wave is given by

$$\vec{\Pi}_{dir} = \frac{e^{ikr}}{4\epsilon\pi r} \hat{y} \quad (2)$$

We decompose this into plane waves and for a given plane wave the Hertz potential can be written as [9]

$$\vec{\Pi}_{inc} = \frac{ik}{8\epsilon\pi^2} \tilde{\Pi} \hat{y} \quad (3)$$

where

$$\tilde{\Pi} = e^{ikz_0 \cos \alpha} e^{ik(x \sin \alpha \cos \beta + y \sin \alpha \sin \beta - z \cos \alpha)} \quad (4)$$

The electric and magnetic fields can be computed by using the formula,

$$\begin{aligned} \vec{E} &= \vec{\nabla}(\vec{\nabla} \cdot \vec{\Pi}) + k^2 \vec{\Pi} \\ \vec{H} &= \frac{k^2}{i\omega\mu} (\vec{\nabla} \times \vec{\Pi}) \end{aligned} \quad (5)$$

where, ω is the angular frequency of radiation and μ is the permeability of medium.

For an incident wave vector given by

$$\vec{k}_i = k[\sin \alpha \cos \beta \hat{x} + \sin \alpha \sin \beta \hat{y} - \cos \alpha \hat{z}] \quad (6)$$

the unit normal $\hat{\eta}$ to the plane of incidence is given by

$$\hat{\eta} = l\hat{x} + m\hat{y} + n\hat{z}. \quad (7)$$

We have $\vec{k}_i \perp \hat{\eta}$ and $\hat{z} \perp \hat{\eta}$. This leads to $\hat{\eta} = (-\sin \beta \hat{x} + \cos \beta \hat{y})$. The incident electric and magnetic fields in the far zone, $r \gg \lambda$, are given by [9]

$$\begin{aligned}\vec{E}_i &= \frac{ik^3}{8\epsilon\pi^2} \tilde{\Pi} [-\sin^2 \alpha \cos \beta \sin \beta \hat{x} + (1 - \sin^2 \alpha \sin^2 \beta) \hat{y} + (\sin \alpha \sin \beta \cos \alpha) \hat{z}] \\ \vec{H}_i &= \frac{ik^2\omega}{8\pi^2} \tilde{\Pi} [\cos \alpha \hat{x} + (\cos \beta \sin \alpha) \hat{z}]\end{aligned}\quad (8)$$

We split these into components perpendicular and parallel to the plane of incidence, i.e.,

$$\begin{aligned}\vec{E}_q &= \vec{E}_q^s + \vec{E}_q^p \\ \vec{H}_q &= \vec{H}_q^s + \vec{H}_q^p\end{aligned}\quad (9)$$

For the electric (magnetic) field, \perp and \parallel components are denoted by the superscripts s (p) and p (s), respectively.

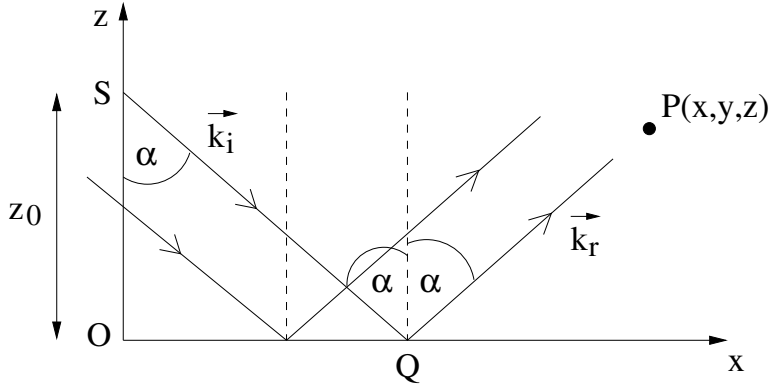


FIG. 1. Reflection from a flat surface: the dipole source is located at $S(0, 0, z_0)$ and the detector is located at P whose position vector is $\vec{r} = (x, y, z)$ with respect to the origin O . A plane wave for which \vec{k}_i makes an angle $\pi - \alpha$ with the z axis is shown. The point Q is the position on the flat surface where the wave vector \vec{k}_i directed from S strikes the surface.

The s and p components of \vec{E}_i can be expressed as:

$$\vec{E}_i^s = \hat{\eta}[\vec{E}_i \cdot \hat{\eta}] = \frac{ik^3}{8\epsilon\pi^2} \tilde{\Pi} (-\cos \beta \sin \beta \hat{x} + \cos^2 \beta \hat{y}) \quad (10)$$

$$\vec{E}_i^p = \frac{ik^3}{8\epsilon\pi^2} \tilde{\Pi} (\cos^2 \alpha \cos \beta \sin \beta \hat{x} + \cos^2 \alpha \sin^2 \beta \hat{y} + \sin \alpha \cos \alpha \sin \beta \hat{z}). \quad (11)$$

Similarly, for the magnetic field

$$\vec{H}_i^p = [\vec{H}_i \cdot \hat{\eta}] \hat{\eta} = \frac{ik^2\omega}{8\pi^2} \tilde{\Pi} (\cos \alpha \sin^2 \beta \hat{x} - \cos \alpha \cos \beta \sin \beta \hat{y}) \quad (12)$$

$$\vec{H}_i^s = \frac{ik^2\omega}{8\pi^2}\tilde{\Pi}(\cos\alpha\cos^2\beta\hat{x} + \cos\alpha\cos\beta\sin\beta\hat{y} + \sin\alpha\cos\beta\hat{z}). \quad (13)$$

The components of the reflected wave are given by

$$\vec{E}_r^s = f_r^s \frac{ik^3}{8\epsilon\pi^2}\tilde{\Pi}_r(-\cos\beta\sin\beta\hat{x} + \cos^2\beta\hat{y}) \quad (14)$$

$$\vec{E}_r^p = f_r^p \frac{ik^3}{8\epsilon\pi^2}\tilde{\Pi}_r(-\cos^2\alpha\cos\beta\sin\beta\hat{x} - \cos^2\alpha\sin^2\beta\hat{y} + \sin\alpha\cos\alpha\sin\beta\hat{z}) \quad (15)$$

where

$$\tilde{\Pi}_r = e^{ikz_0\cos\alpha} e^{ik(x\sin\alpha\cos\beta+y\sin\alpha\sin\beta+z\cos\alpha)}. \quad (16)$$

Similarly,

$$\vec{H}_r^p = f_r^p \frac{ik^2\omega}{8\pi^2}\tilde{\Pi}_r(\cos\alpha\sin^2\beta\hat{x} - \cos\alpha\cos\beta\sin\beta\hat{y}) \quad (17)$$

and

$$\vec{H}_r^s = f_r^s \frac{ik^2\omega}{8\pi^2}\tilde{\Pi}_r(-\cos\alpha\cos^2\beta\hat{x} - \cos\alpha\cos\beta\sin\beta\hat{y} + \sin\alpha\cos\beta\hat{z}). \quad (18)$$

Here f_r^s and f_r^p are the reflection coefficients which are determined by boundary conditions.

The corresponding transmitted fields \vec{E}_t^s , \vec{E}_t^p , \vec{H}_t^s and \vec{H}_t^p are given by

$$\vec{E}_t^s = f_t^s \frac{ik_1^3}{8\epsilon_1\pi^2}(-\cos\beta_t\sin\beta_t\hat{x} + \cos^2\beta_t\hat{y})\tilde{\Pi}_t \quad (19)$$

$$\vec{E}_t^p = f_t^p \frac{ik_1^3}{8\epsilon_1\pi^2}(\cos^2\alpha_t\cos\beta_t\sin\beta_t\hat{x} + \cos^2\alpha_t\sin^2\beta_t\hat{y} + \cos\alpha_t\sin\alpha_t\sin\beta_t\hat{z})\tilde{\Pi}_t \quad (20)$$

$$\vec{H}_t^p = f_t^p \frac{ik_1^2\omega}{8\pi^2}(\cos\alpha_t\sin^2\beta_t\hat{x} - \cos\alpha_t\cos\beta_t\sin\beta_t\hat{y})\tilde{\Pi}_t, \quad (21)$$

and

$$\vec{H}_t^s = f_t^s \frac{ik_1^2\omega}{8\pi^2}(\cos\alpha_t\cos^2\beta_t\hat{x} + \cos\alpha_t\cos\beta_t\sin\beta_t\hat{y} + \sin\alpha_t\cos\beta_t\hat{z})\tilde{\Pi}_t. \quad (22)$$

where

$$\tilde{\Pi}_t = e^{ikz_0\cos\alpha} e^{ik_1(x\sin\alpha_t\cos\beta_t+y\sin\alpha_t\sin\beta_t-z\cos\alpha_t)} \quad (23)$$

$$\vec{k}_t = k_1[\sin\alpha_t\cos\beta_t\hat{x} + \sin\alpha_t\sin\beta_t\hat{y} - \cos\alpha_t\hat{z}], \quad (24)$$

We next impose the boundary conditions at the interface. We shall assume $\mu = \mu_1$. We obtain

$$k\sin\alpha = k_1\sin\alpha_t, \quad \beta = \beta_t. \quad (25)$$

$$f_r^p = \frac{k_1\cos\alpha - k\cos\alpha_t}{k_1\cos\alpha + k\cos\alpha_t} \quad (26)$$

$$f_t^p = \left(\frac{k}{k_1}\right)^2 \left(\frac{1}{\cos \alpha_t}\right) \frac{2k_1 \cos^2 \alpha}{k_1 \cos \alpha + k \cos \alpha_t}. \quad (27)$$

$$f_r^s = \frac{k \cos \alpha - k_1 \cos \alpha_t}{k \cos \alpha + k_1 \cos \alpha_t} \quad (28)$$

and

$$f_t^s = \left(\frac{k}{k_1}\right)^2 \frac{2k_1 \cos \alpha}{k_1 \cos \alpha_t + k \cos \alpha}. \quad (29)$$

Using the above Fresnel coefficients the y components (H-Pol) of the reflected and transmitted electric field at $y = 0$ can be expressed as

$$E_{r,y} = \frac{ik^3}{8\epsilon\pi^2} \int_0^{2\pi} \int_0^{\frac{\pi}{2}-i\infty} \tilde{\Pi}_r(f_r^s \cos^2 \beta - f_r^p \cos^2 \alpha \sin^2 \beta) \sin \alpha d\alpha d\beta. \quad (30)$$

$$E_{t,y} = \frac{ik_1^3}{8\epsilon_1\pi^2} \int_0^{2\pi} \int_0^{\frac{\pi}{2}-i\infty} \tilde{\Pi}_t(f_t^s \cos^2 \beta_t + f_t^p \cos^2 \alpha_t \sin^2 \beta_t) \sin \alpha d\alpha d\beta. \quad (31)$$

Using Eq. 30 we can compute the y -component of the total reflected field for a flat reflecting surface. The resulting value of the reflection coefficient is found to be same as that for Fresnel reflection independent of frequency.

III. REFLECTION AND TRANSMISSION ON A SPHERICAL SURFACE USING LOCAL PLANE WAVE APPROXIMATION

In this section we introduce a rigorous formalism to handle reflection of spherical waves from a spherical surface. The radius of curvature is assumed to be much larger than the wavelength. We again decompose the incident wave into plane waves (see Eq. 1). In an earlier calculation [9] we had assumed that the reflected wave corresponding to each incident plane wave is also a plane wave. This is a reasonable approximation since the curvature is very small. However by direct comparison with HiCal observations the theoretical results were found to disagree with data for small elevation angles. In the present paper we assume that the reflected wave is only locally a plane wave. We explain this in Fig. 2. Consider an incident plane wave with wave vector \vec{k}_i which reflects off the curved surface. In the figure we have shown reflection from two points C and C' . For the point C the reflected wave vector \vec{k}_r can be obtained by requiring that the reflection takes place from a plane tangent to the surface at C . In the neighbourhood of the vector \vec{k}_r the wave is assumed to be locally a plane wave. The reflected wave vector corresponding to point C' , however, points in a different direction. Hence globally the wave fronts are not plane. For a particular incident

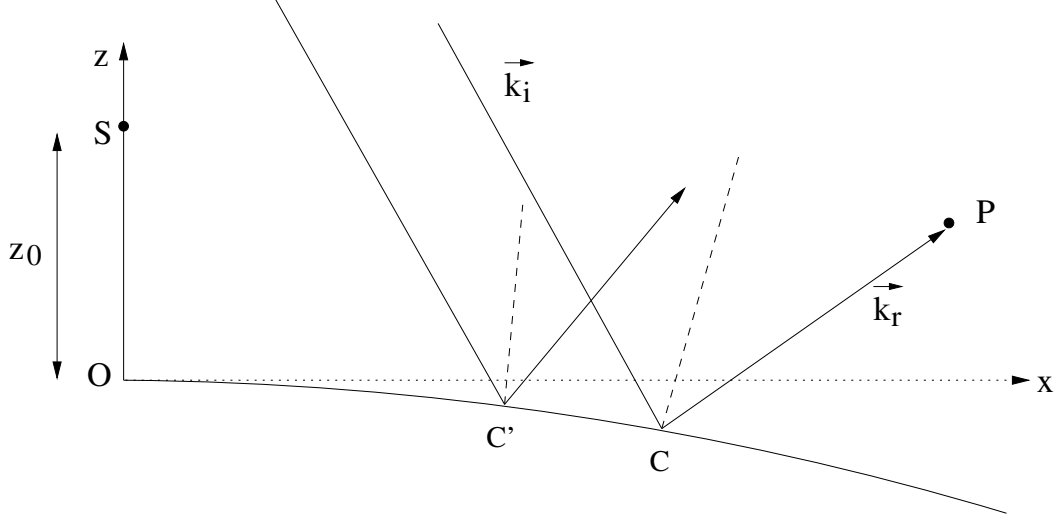


FIG. 2. Here S is the source and P the detector. A plane wave with wave vector \vec{k}_i reflects off the spherical surface. Here we show its reflection at two points C and C' . The reflected wave vector (such as \vec{k}_r) at any point (for example C) is obtained by constructing a tangent plane at that point. We obtain \vec{k}_i by demanding that \vec{k}_r points towards P . Notice that different wave vectors corresponding to this incident plane wave which strike the surface at different points reflect off in different directions. Hence the reflected wave is not a plane wave. We also show a wave vector for this plane wave which reflects off at point C' .

plane wave we need to choose the incident wave vector for which the reflected wave vector \vec{k}_r points towards the observation point P . We follow the same procedure for all plane waves and add the total contribution at the observation point.

We first need to determine the relationship between the angles α and α' for a particular plane wave, where α' is the reflection angle as shown in Fig. 3. For this purpose it is convenient to shift the coordinate system to O' . The detector $P(x, 0, z)$ is located vertically above this point at altitude h' . We identify a point Q on the surface of Earth such that the reflected wave vector \vec{k}_r corresponding to the incident wave vector \vec{k}_i at this point is directed towards the detector at P . We start with a reflected wave vector \vec{k}_r and find the corresponding incident wave vector \vec{k}_i as shown in Fig. 3.

For a given point of observation $P(x, 0, z)$ the angle ξ , defined in Fig. 3, is given by $\tan \xi = \frac{x}{R+z}$, where R is the radius of Earth. We first rotate our coordinate system about the y axis by angle ξ and obtain coordinate system $x'' - y'' - z''$. The z'' axis meets the

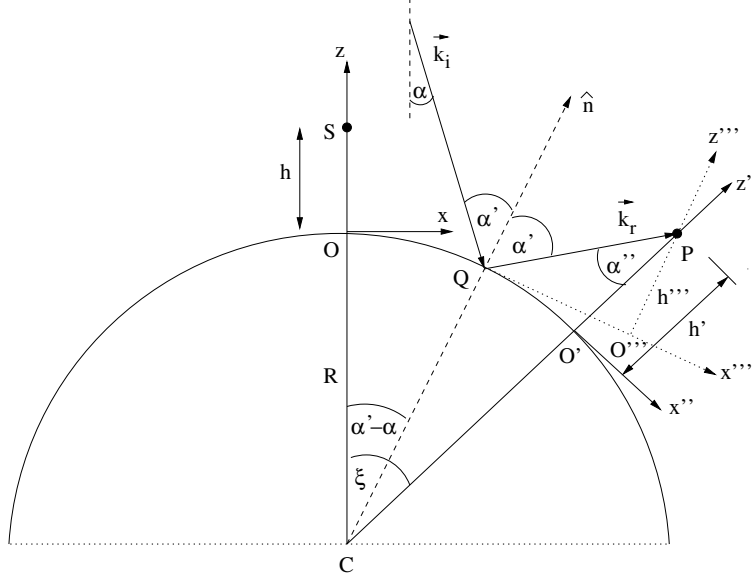


FIG. 3. The source is a horizontal dipole radiator located at $S(0,0,h)$ on the z axis and the detector is at P . The point of reflection Q for a particular plane wave is chosen such that the reflected wave vector \vec{k}_r points towards P . The incident wave vector is denoted by \vec{k}_i . Here C is the centre of Earth and R is the radius of Earth. The position vector of O' with respect to O is \vec{r}_0 . The normal to the surface at Q is denoted by \hat{n} which is parallel to the z''' axes. Angle of reflection and angle of transmission at point Q are α' and α_t' (not shown in figure) respectively.

surface of Earth at the point O' . We choose O' as our reference point for further calculations. The rotation matrix corresponding to this is

$$R_y(\xi) = \begin{pmatrix} \cos \xi & 0 & -\sin \xi \\ 0 & 1 & 0 \\ \sin \xi & 0 & \cos \xi \end{pmatrix} \quad (32)$$

The unit vectors in this new coordinate system are related to the unit vectors in $x - y - z$ by

$$\begin{aligned} \hat{x}'' &= \cos \xi \hat{x} - \sin \xi \hat{z} \\ \hat{y}'' &= \hat{y} \\ \hat{z}'' &= \sin \xi \hat{x} + \cos \xi \hat{z} \end{aligned} \quad (33)$$

Next we rotate the coordinate system $(x'' - y'' - z'')$ about the z'' axis by an angle $\tilde{\beta}$. This

leads to the rotation matrix as,

$$R_{z''}(\tilde{\beta}) = \begin{pmatrix} \cos \tilde{\beta} & \sin \tilde{\beta} & 0 \\ -\sin \tilde{\beta} & \cos \tilde{\beta} & 0 \\ 0 & 0 & 1 \end{pmatrix} \quad (34)$$

Note that the rotation about z'' axis by angle $\tilde{\beta}$ enables us to get the contribution from all locally plane waves that reach the detector at P by use of cylindrical symmetry. Due to the second rotation, we finally obtain our coordinate system $(x' - y' - z')$ such that

$$\begin{aligned} \hat{x}' &= \cos \tilde{\beta} \hat{x}'' + \sin \tilde{\beta} \hat{y}'' \\ \hat{y}' &= -\sin \tilde{\beta} \hat{x}'' + \cos \tilde{\beta} \hat{y}'' \\ \hat{z}' &= \hat{z}'' \end{aligned} \quad (35)$$

Now the overall rotation matrix is given by, $Rot_1 = R_{z''}(\tilde{\beta})R_y(\xi)$

$$Rot_1 = \begin{pmatrix} \cos \xi \cos \tilde{\beta} & \sin \tilde{\beta} & -\sin \xi \cos \tilde{\beta} \\ -\cos \xi \sin \tilde{\beta} & \cos \tilde{\beta} & \sin \xi \sin \tilde{\beta} \\ \sin \xi & 0 & \cos \xi \end{pmatrix} \quad (36)$$

Next we write the incident wave vector in the new coordinate system as,

$$\vec{k}'_i = Rot_1 \cdot \vec{k}_i = k'_x \hat{x}' + k'_y \hat{y}' + k'_z \hat{z}' \quad (37)$$

Using 6 and 36 we obtain the components of incident wave vector in $x' - y' - z'$ coordinate system as

$$\begin{aligned} k'_x &= k((\sin \alpha \cos \beta \cos \xi + \cos \alpha \sin \xi) \cos \tilde{\beta} + \sin \alpha \sin \beta \sin \tilde{\beta}) \\ k'_y &= k((- \sin \alpha \cos \beta \cos \xi - \cos \alpha \sin \xi) \sin \tilde{\beta} + \sin \alpha \sin \beta \cos \tilde{\beta}) \\ k'_z &= k((- \sin \alpha \cos \beta \sin \xi + \cos \alpha \cos \xi) \sin \tilde{\beta} + \sin \alpha \sin \beta \cos \tilde{\beta}) \end{aligned} \quad (38)$$

Since \vec{k}'_i lies in the $x' - z'$ plane which is our plane of incidence, we must set y' component of \vec{k}'_i as zero. This leads to the expression of $\tilde{\beta}$ as

$$\tan \tilde{\beta} = \frac{\sin \alpha \sin \beta}{\sin \alpha \cos \beta \cos \xi + \cos \alpha \sin \xi} \quad (39)$$

We introduce a new parameter $\tilde{\alpha}$ such that

$$\cos \tilde{\alpha} = (\cos \alpha \cos \xi - \sin \alpha \cos \beta \sin \xi) \quad (40)$$

and

$$\sin \tilde{\alpha} = ((\sin \alpha \cos \xi \cos \beta + \cos \alpha \sin \xi)^2 + (\sin \alpha \sin \beta)^2)^{\frac{1}{2}} \quad (41)$$

Using 38–41 we simplify the expression for incident wave vector \vec{k}'_i and express it as

$$\vec{k}'_i = k(\sin \tilde{\alpha} \hat{x}' - \cos \tilde{\alpha} \hat{z}') \quad (42)$$

The reflected wave vector in the new coordinate system is given by,

$$\vec{k}'_r = Rot_1 \cdot \vec{k}_r = k(\sin \alpha'' \hat{x}' + \cos \alpha'' \hat{z}') \quad (43)$$

Similarly, the transmitted wave vector in the new coordinate system is given by,

$$\vec{k}'_t = Rot_1 \cdot \vec{k}_t = k_1(\sin \tilde{\alpha}_t \hat{x}' - \cos \tilde{\alpha}_t \hat{z}') \quad (44)$$

The normal to the spherical surface at Q is given by

$$\hat{n} = \cos(\xi - (\alpha' - \alpha))\hat{z}' - \sin(\xi - (\alpha' - \alpha))\hat{x}' \quad (45)$$

From 42–44, we see that the incident, reflected and transmitted wave vectors lie in the same plane. The normal \hat{n} must also lie in the $x' - z'$ plane to satisfy the laws of reflection at the interface between air and ice. Using the condition $-\hat{n} \cdot \vec{k}'_i = \hat{n} \cdot \vec{k}'_r$, we get a relation between angle of reflection α' and angle α as

$$\alpha'' = -2\xi + 2\alpha' - 2\alpha + \tilde{\alpha} \quad (46)$$

From the geometry (see Fig. 3) we derive

$$\sin \alpha' = \frac{R + h'}{R} \sin \alpha'' \quad (47)$$

Using 40, 46 and 47 we numerically solve this equation in order to determine α' as a function of α for a given observation point P (see Fig.3). The reference point O' is located at \vec{r}_0 from the origin $O(0, 0, 0)$. The point of reflection Q and the observation point P are located at \vec{r}'_s and \vec{r}' respectively with respect to O' . From the geometry (see Fig. 3) we obtain the expression for \vec{r}'_0 , \vec{r}'_s and \vec{r}' as

$$\vec{r}' = h' \hat{z}'' = h' \hat{z}' \quad (48)$$

$$R \hat{z} + \vec{r}_0 = \vec{r}_2 = R(\sin \xi \hat{x} + \cos \xi \hat{z})$$

or

$$\vec{r}_0 = R(\cos \xi - 1) \hat{z} + R \sin \xi \hat{x} \quad (49)$$

and

$$\vec{r}'_s = \vec{r}_1 - \vec{r}_2 = -R \sin(\xi - \alpha' + \alpha) \hat{x}'' - R(1 - \cos(\xi - \alpha' + \alpha)) \hat{z}'' \quad (50)$$

For $\tilde{\beta}=\beta=0$, we get

$$\xi = 2\alpha' - \alpha - \alpha''$$

or

$$\xi - \alpha' + \alpha = \alpha' - \alpha''. \quad (51)$$

Using Eq. 50 and 51, we obtain the expression for \vec{r}'_s as

$$\vec{r}'_s = -R \sin(\alpha' - \alpha'') \hat{x}' - R(1 - \cos(\alpha' - \alpha'')) \hat{z}', \quad (52)$$

which is valid for any $\tilde{\beta}$. The exponential factor for the incident plane wave is derived for the spherical geometry using the same method as in the case of flat geometry. We express it as,

$$\begin{aligned} \tilde{\Pi}_{S,i} &= \exp \left[i \vec{k}'_i \cdot (\vec{r}' + \vec{r}_0 - h \hat{z}) \right] \\ &= \exp \left[ik(x \sin \alpha \cos \beta + y \sin \alpha \sin \beta + (h - z) \cos \alpha) \right]. \end{aligned} \quad (53)$$

From geometry (Fig. 3) we find the expression for h' as

$$h' = R \left[\left(1 + \frac{z}{R} \right)^2 + \left(\frac{x}{R} \right)^2 \right]^{\frac{1}{2}} - R. \quad (54)$$

Now we obtain the exponential factor for the reflected wave by applying the boundary conditions at the point Q whose position vector with respect to O' is \vec{r}'_s .

$$\vec{k}'_i \cdot \vec{r}'_s + \vec{k}'_i \cdot (\vec{r}_0 - h \hat{z}) = \vec{k}'_r \cdot \vec{r}'_s + D \quad (55)$$

This fixes the value of D and the resulting expression for $\tilde{\Pi}_{S,r}$ is given by

$$\begin{aligned} \tilde{\Pi}_{S,r} &= \exp[i(\vec{k}'_r \cdot \vec{r}' + D)] \\ &= \exp[i(\vec{k}'_r \cdot \vec{r}' + \vec{k}'_i \cdot \vec{r}'_s + \vec{k}'_i \cdot (\vec{r}_0 - h \hat{z}) - \vec{k}'_r \cdot \vec{r}'_s)]. \end{aligned}$$

This leads to

$$\tilde{\Pi}_{S,r} = \exp[ik((R + h') \cos \alpha'' + (R + h) \cos \alpha - R \cos \alpha' - R \cos(\alpha' - \alpha'' - \tilde{\alpha}))] \quad (56)$$

Similarly, we determine the exponential factor for the transmitted wave from the geometry (see Fig. 3). We express it as

$$\tilde{\Pi}_{S,t} = e^{i\vec{k}'_i \cdot \vec{\Delta}'} e^{i\vec{k}'_i \cdot \vec{r}'} \quad (57)$$

where $e^{i\vec{k}'_i \cdot \vec{\Delta}'}$ is the constant term appearing in both $\tilde{\Pi}_{S,i}$ and $\tilde{\Pi}_{S,t}$. As in the case of flat geometry, this term is proportional to k and not k_1 . We write the electric field components in the $(x' - y' - z')$ coordinate system as

$$\begin{aligned} \vec{E}'_i &= Rot_1 \cdot \vec{E}_i = \frac{ik^3}{8\epsilon\pi^2} \tilde{\Pi}_{S,i} [\sin \tilde{\beta} \cos^2 \tilde{\alpha} \hat{x}' + \cos \tilde{\beta} \hat{y}' + \cos \tilde{\alpha} \sin \alpha \sin \tilde{\beta} \hat{z}'] \\ \vec{H}'_i &= Rot_1 \cdot \vec{H}_i = \frac{ik^2\omega}{8\pi^2} \tilde{\Pi}_{S,i} [\cos \tilde{\alpha} \cos \tilde{\beta} \hat{x}' - \cos \tilde{\alpha} \sin \tilde{\beta} \hat{y}' + \sin \tilde{\alpha} \cos \tilde{\beta} \hat{z}'] \end{aligned} \quad (58)$$

A. Deriving Reflection and Transmission Coefficients and Comparison with HiCal Data

As explained in earlier sections the basic idea of the local plane wave approximation is that we demand that the reflected wave vector \vec{k}_r corresponding to any incident plane wave points towards the detector located at P . For all such vectors we determine the incident wave vectors \vec{k}_i and eventually need to integrate over the contributions from all the plane waves. In order to determine the reflected and transmitted waves we follow the same procedure as before [9]. For each plane wave we determine the tangent plane at the point of reflection Q . The tangent plane acts as the flat reflecting surface and now we can use the procedure for flat surface to determine the Fresnel coefficients. As in [9] we transform to a coordinate system $x''' - y''' - z'''$ in which this surface is the $x''' - y'''$ plane. Using the reflection coefficients, we compute the electric and magnetic field components for each plane wave in the new coordinate system. Since the new coordinate system is not fixed rather it depends on the plane wave under consideration, we transform our fields back to the original frame and integrate over all plane waves to get the total field.

For a given plane wave, let the point Q be located at (x_s, y_s, z_s) with respect to origin $O(0, 0, 0)$. We identify the tangent plane at this point and choose a new coordinate system $(x''' - y''' - z''')$ such that it satisfies the following conditions:

1. The coordinates of Q in this system are $(x_s''', 0, 0)$.
2. The observation point P lies on the z''' axis at a height h''' above the new reference point O''' .
3. The unit vector \hat{n} , normal to the tangent plane at Q is parallel to the z''' axis (see Fig. 3).

We have

$$\hat{n} = -\sin \psi \hat{x}' + \cos \psi \hat{z}' \quad (59)$$

where

$$\psi = \xi - \alpha' + \alpha \quad (60)$$

The final rotation matrix in order to transform from $x' - y' - z'$ to $x''' - y''' - z'''$ coordinate system is given by,

$$R_{y'}(\psi) = \begin{pmatrix} \cos \psi & 0 & \sin \psi \\ 0 & 1 & 0 \\ -\sin \psi & 0 & \cos \psi \end{pmatrix} \quad (61)$$

The unit vectors in this coordinate system are

$$\begin{aligned} \hat{x}''' &= \cos \psi \hat{x}' + \sin \psi \hat{z}' \\ \hat{y}''' &= \hat{y}' \\ \hat{z}''' &= -\sin \psi \hat{x}' + \cos \psi \hat{z}' \end{aligned} \quad (62)$$

Incorporating all three rotations, we obtain the full rotation matrix using Eq.(36) and Eq.(61) as

$$Rot = R_{y'}(\psi) Rot_1 = R_{y'}(\psi) R_{z''}(\tilde{\beta}) R_y(\xi) \quad (63)$$

We find the incident, reflected and transmitted wave vectors in the new coordinate system as

$$\begin{aligned} \vec{k}_i''' &= k[\sin(\tilde{\alpha} - \psi)\hat{x}''' - \cos(\tilde{\alpha} - \psi)\hat{z}'''] \\ \vec{k}_r''' &= k[\sin(\alpha'' + \psi)\hat{x}''' + \cos(\alpha'' + \psi)\hat{z}'''] \\ \vec{k}_t''' &= k_1[\sin(\tilde{\alpha}_t - \psi)\hat{x}''' - \cos(\tilde{\alpha}_t - \psi)\hat{z}'''] \end{aligned} \quad (64)$$

We have simplified the expression for transmitted wave vector \vec{k}_t''' using

$$\cos \tilde{\alpha}_t = (\cos \alpha_t \cos \xi - \sin \alpha_t \cos \beta_t \sin \xi) \quad (65)$$

The electric and magnetic field expressions in the $(x''' - y''' - z''')$ are obtained as

$$\begin{aligned}
\vec{E}_i''' &= R_{y'}(\psi)\vec{E}_i' \\
&= \frac{ik^3}{8\epsilon\pi^2}\tilde{\Pi}_{S,i}[(\sin\tilde{\beta}\cos^2\tilde{\alpha}\cos\psi + \sin\alpha\cos\tilde{\alpha}\sin\beta\sin\psi)\hat{x}''' + \cos\tilde{\beta}\hat{y}''' \\
&\quad + (\sin\alpha\cos\tilde{\alpha}\sin\beta\cos\psi - \cos^2\tilde{\alpha}\sin\tilde{\beta}\sin\psi)\hat{z}''']
\end{aligned} \tag{66}$$

$$\begin{aligned}
\vec{H}_i''' &= R_{y'}(\psi)\vec{H}_i' \\
&= \frac{ik^2\omega}{8\pi^2}\tilde{\Pi}_{S,i}[\cos\tilde{\beta}\cos(\tilde{\alpha} - \psi)\hat{x}''' - \cos\tilde{\alpha}\sin\tilde{\beta}\hat{y}''' \\
&\quad + \cos\tilde{\beta}\sin(\tilde{\alpha} - \psi)\hat{z}''']
\end{aligned} \tag{67}$$

Now we use the same method as in the case of flat geometry to find the s and p components of E_q''' and H_q''' (where the subscript q designates the incident, reflected or transmitted waves).

We derive the reflection and transmission coefficients by imposing boundary conditions at Q i.e. $z_s''' = 0$. We find the unit vector normal to the plane of incidence corresponding to wave vector \vec{k}_i''' as

$$\hat{\eta} = l\hat{x}''' + m\hat{y}''' + n\hat{z}''' \tag{68}$$

The vector \vec{k}_i''' and \hat{z}''' lie in the plane of incidence and hence are perpendicular to $\hat{\eta}$. This implies that $n = 0$ and $(l\hat{x}''' + m\hat{y}''' + n\hat{z}''') \cdot \vec{k}_i''' = 0$. The resulting unit vector $\hat{\eta}$ perpendicular to the plane of incidence is given by,

$$\hat{\eta} = \hat{y}''' \tag{69}$$

Now we write the s and p components of incident electric field as

$$\begin{aligned}
\vec{E}_i'''(s) &= (\vec{E}_i''' \cdot \hat{\eta})\hat{\eta} = \frac{ik^3}{8\epsilon\pi^2}\tilde{\Pi}_{S,i}\cos\tilde{\beta}\hat{y}''' \\
\vec{E}_i'''(p) &= \vec{E}_i''' - \vec{E}_i'''(s) = \frac{ik^3}{8\epsilon\pi^2}\tilde{\Pi}_{S,i}[(\sin\tilde{\beta}\cos^2\tilde{\alpha}\cos\psi + \sin\alpha\cos\tilde{\alpha}\sin\beta\sin\psi)\hat{x}''' \\
&\quad + (\sin\alpha\cos\tilde{\alpha}\sin\beta\cos\psi - \cos^2\tilde{\alpha}\sin\tilde{\beta}\sin\psi)\hat{z}''']
\end{aligned} \tag{70}$$

Similarly the incident magnetic field components can be written as

$$\vec{H}_i'''(p) = (\vec{H}_i''' \cdot \hat{\eta})\hat{\eta} = \frac{ik^2\omega}{8\pi^2}\tilde{\Pi}_{S,i}[-\cos\tilde{\alpha}\sin\tilde{\beta}\hat{y}''']$$

$$\vec{H}_i^{m(s)} = \vec{H}_i^m - \vec{H}_i^{m(p)} = \frac{ik^2\omega}{8\pi^2} \tilde{\Pi}_{S,i} [\cos \tilde{\beta} \cos(\tilde{\alpha} - \psi) \hat{x}''' + \cos \tilde{\beta} \sin(\tilde{\alpha} - \psi) \hat{z}'''] \quad (71)$$

The s and p components of reflected electric field are obtained as

$$\begin{aligned} \vec{E}_r^{m(s)} &= f_r^{(s)} \frac{ik^3}{8\epsilon\pi^2} \tilde{\Pi}_{S,r} [\cos \tilde{\beta} \hat{y}'''], \\ \vec{E}_r^{m(p)} &= f_r^{(p)} \frac{ik^3}{8\epsilon\pi^2} \tilde{\Pi}_{S,r} [-(\sin \tilde{\beta} \cos^2 \tilde{\alpha} \cos \psi + \sin \alpha \cos \tilde{\alpha} \sin \beta \sin \psi) \hat{x}''' \\ &\quad + (\sin \alpha \cos \tilde{\alpha} \sin \beta \cos \psi - \cos^2 \tilde{\alpha} \sin \tilde{\beta} \sin \psi) \hat{z}'''] \end{aligned} \quad (72)$$

Similarly, for the reflected magnetic field components we write

$$\begin{aligned} \vec{H}_r^{m(p)} &= f_r^{(p)} \frac{ik^2\omega}{8\pi^2} \tilde{\Pi}_{S,r} [-\cos \tilde{\alpha} \sin \tilde{\beta} \hat{y}'''], \\ \vec{H}_r^{m(s)} &= f_r^{(s)} \frac{ik^2\omega}{8\pi^2} \tilde{\Pi}_{S,r} [-\cos \tilde{\beta} \cos(\tilde{\alpha} - \psi) \hat{x}''' + \cos \tilde{\beta} \sin(\tilde{\alpha} - \psi) \hat{z}'''] \end{aligned} \quad (73)$$

where, $f_r^{(s)}$ and $f_r^{(p)}$ are fresnel coefficients corresponding to s and p component of reflected fields.

The corresponding transmitted field $\vec{E}_t^{m(s)}$, $\vec{E}_t^{m(p)}$, $\vec{H}_t^{m(s)}$ and $\vec{H}_t^{m(p)}$ can be written as

$$\begin{aligned} \vec{E}_t^{m(s)} &= f_t^{(s)} \frac{ik_1^3}{8\epsilon_1\pi^2} \tilde{\Pi}_{S,t} [\cos \tilde{\beta}_t \hat{y}'''], \\ \vec{E}_t^{m(p)} &= \vec{E}_t^m - \vec{E}_t^{m(s)} \\ &= f_t^{(p)} \frac{ik_1^3}{8\epsilon_1\pi^2} \tilde{\Pi}_{S,t} [(\sin \tilde{\beta}_t \cos^2 \tilde{\alpha}_t \cos \psi + \sin \alpha_t \cos \tilde{\alpha}_t \sin \beta_t \sin \psi) \hat{x}''' \\ &\quad + (\sin \alpha_t \cos \tilde{\alpha}_t \sin \beta_t \cos \psi - \cos^2 \tilde{\alpha}_t \sin \tilde{\beta}_t \sin \psi) \hat{z}'''] \end{aligned} \quad (74)$$

Similarly the transmitted magnetic field components can be written as

$$\begin{aligned} \vec{H}_t^{m(p)} &= f_t^{(p)} \frac{ik_1^2\omega}{8\pi^2} \tilde{\Pi}_{S,t} [-\cos \tilde{\alpha}_t \sin \tilde{\beta}_t \hat{y}'''], \\ \vec{H}_t^{m(s)} &= \vec{H}_t^m - \vec{H}_t^{m(p)} = f_t^{(s)} \frac{ik_1^2\omega}{8\pi^2} \tilde{\Pi}_{S,t} [\cos \tilde{\beta}_t \cos(\tilde{\alpha}_t - \psi) \hat{x}''' \\ &\quad + \cos \tilde{\beta}_t \sin(\tilde{\alpha}_t - \psi) \hat{z}'''] \end{aligned} \quad (75)$$

We impose the boundary conditions at $z_s''' = 0$ on each components in order to determine the reflection coefficients. We use the same procedure as described in [9]. The exponential factors lead to the standard conditions:

$$\begin{aligned} k \sin(\tilde{\alpha} - \psi) &= k_1 \sin(\tilde{\alpha}_t - \psi) \\ \tilde{\beta}_t &= \tilde{\beta} \end{aligned} \quad (76)$$

The continuity of electric field components \parallel to the surface imply that

$$\vec{E}_{t,x}'''(p) = \vec{E}_{i,x}'''(p) + \vec{E}_{r,x}'''(p)$$

The components \perp to the surface follow:

$$\epsilon_1 \vec{E}_{t,z}'''(p) = \epsilon [\vec{E}_{i,z}'''(p) + \vec{E}_{r,z}'''(p)]$$

The component of magnetic field \perp to the surface are continuous at the interface and the parallel components satisfy,

$$\mu_1 \vec{H}_{t,y}'''(p) = \mu \left[\vec{H}_{i,y}'''(p) + \vec{H}_{r,y}'''(p) \right].$$

Here we shall assume $\mu_1 = \mu$. These conditions lead to:

$$(1 - f_r'(p)) = f_t'(p) \frac{k_1 \cos \tilde{\alpha}_t \cos(\tilde{\alpha}_t - \psi)}{k \cos \tilde{\alpha} \cos(\tilde{\alpha} - \psi)} \quad (77)$$

$$(1 + f_r'(p)) = f_t'(p) \frac{k_1^3 \cos \tilde{\alpha}_t \sin(\tilde{\alpha}_t - \psi)}{k^3 \cos \tilde{\alpha} \sin(\tilde{\alpha} - \psi)} = f_t'(p) \frac{k_1^2 \cos \tilde{\alpha}_t}{k^2 \cos \tilde{\alpha}} \quad (78)$$

Solving Eqs. 77 and 78 we obtain

$$f_r'(p) = \frac{k_1 \cos(\tilde{\alpha} - \psi) - k \cos(\tilde{\alpha}_t - \psi)}{k_1 \cos(\tilde{\alpha} - \psi) + k \cos(\tilde{\alpha}_t - \psi)},$$

and

$$f_t'(p) = \left(\frac{k}{k_1} \right)^2 \left(\frac{1}{\cos \tilde{\alpha}_t} \right) \frac{2k_1 \cos(\tilde{\alpha} - \psi) \cos \tilde{\alpha}}{k_1 \cos(\tilde{\alpha} - \psi) + k \cos(\tilde{\alpha}_t - \psi)} \quad (79)$$

Next we impose boundary conditions on the components \perp to the plane of incidence. These leads to

$$\vec{E}_{t,y}'''(s) = \vec{E}_{i,y}'''(s) + \vec{E}_{r,y}'''(s)$$

and

$$\mu_1 \vec{H}_{t,x}'''(p) = \mu \left[\vec{H}_{i,x}'''(p) + \vec{H}_{r,x}'''(p) \right]$$

The z component of the electric field does not lead to a new condition. These conditions imply

$$(1 + f_r'(s)) = f_t'(s) \frac{k_1}{k} \quad (80)$$

and

$$(1 - f_r'(s)) = f_t'(s) \frac{k_1^2 \cos(\tilde{\alpha}_t - \psi)}{k^2 \cos(\tilde{\alpha} - \psi)} \quad (81)$$

Solving Eqs. 80 and 81 we obtain,

$$f_r^{(s)} = \frac{k \cos(\tilde{\alpha} - \psi) - k_1 \cos(\tilde{\alpha}_t - \psi)}{k \cos(\tilde{\alpha} - \psi) + k_1 \cos(\tilde{\alpha}_t - \psi)},$$

and

$$f_t^{(s)} = \left(\frac{k}{k_1}\right)^2 \frac{2k_1 \cos(\tilde{\alpha} - \psi)}{k \cos(\tilde{\alpha} - \psi) + k_1 \cos(\tilde{\alpha}_t - \psi)} \quad (82)$$

Using the above coefficients we now write the reflected electric field expression for each plane wave by adding s and p components of E_r''' as shown in section II .

$$\vec{E}_r''' = \vec{E}_r'''^{(s)} + \vec{E}_r'''^{(p)} \quad (83)$$

Finally we transform back to the fixed coordinate system $(x - y - z)$. Using the inverse of the rotation matrix Rot , we write the expression for reflected electric field in the original coordinate system as

$$\vec{E}_r = Rot^{-1} \cdot \vec{E}_r''' \quad (84)$$

Since we are interested only in the perpendicular component, we consider only the y-component of the electric field. For each plane wave we obtain the y- component of \vec{E}_r as

$$E_{r,y} = \frac{ik^3}{8\epsilon\pi^2} \tilde{\Pi}_{S,r} \left[f_r^{(s)} \cos^2 \tilde{\beta} - f_r^{(p)} \cos \tilde{\alpha} \cos(\tilde{\alpha} - 2\psi) \sin^2 \tilde{\beta} \right] \quad (85)$$

We include the corrections due to the roughness of ice surface by using the model [9, 16]

$$F_{rough}(k, \rho, \theta) = \exp \left[-2k^2 \sigma_h(\rho_\perp)^2 \cos^2 \theta_z \right] . \quad (86)$$

Here θ_z is the angle relative to normal at the point of specular reflection, $\rho_\perp^2 = x_\perp^2 + y_\perp^2$, x_\perp, y_\perp represent the coordinates with origin at the specular point and

$$\sigma_h(L) = \sigma_h(L_0) \left(\frac{L}{L_0} \right)^H . \quad (87)$$

We choose the parameters $L_0 = 150$ m, $\sigma_h(150m) = 0.041m$ and $H = 0.65$ which are found to provide reasonable agreement with data for all elevation angles. Including the roughness factor $F_{rough} = F(k, \rho, \theta)$ in our calculation [9], we compute the y-component of total reflected field. The resulting total reflected electric field can be written as

$$E_{(r,total),y} = \int_0^{2\pi} \int_0^{\frac{\pi}{2} - i\infty} F_{rough} E_{r,y} \sin \alpha d\alpha d\beta. \quad (88)$$

The integral gets dominant contribution from regions close to the specular point. Hence we integrate only over a small neighbourhood of this point. We choose refractive index of ice $n = 1.4$ and compute Eq. 88 for several frequencies in the range 200 MHz-650 MHz. The power reflection ratio shows a mild dependence on frequency. This is shown in Fig. 4. We see that the ratio first shows a mild increase with frequency and then starts to decrease. The error bars shown arise since the reflected power shows rapid fluctuations as a function of frequency as well as the angle of incidence. This was also seen in the formalism used in [9] for a spherical surface. The level of fluctuations depend on the roughness parameters and get reduced with increase in the roughness contribution. In the earlier formalism [9], they were found to be negligible for the roughness parameters used in this calculation. This is not the case for the present formalism. We also find that the amplitude of the fluctuations becomes very large for small elevation angles as well as for small frequencies. In Fig. 4 we show the ratio of reflected to direct power, averaged over a small neighbourhood of the chosen frequency. The corresponding standard deviation gives the error. We also find that the ratio increases slightly with the refractive index of ice for large values of θ_z .

In Fig. 5 we show power reflection ratio as a function of the elevation angle ($90^\circ - \theta_z$). This is computed by taking the average of a large number of points (approximately 15) over the frequency range 200-650 MHz. The blue circles show the calculated power ratio and the dashed curve a smooth fit through the calculated points. Each of these data points have an error arising from the fluctuations in the theoretical calculation as a function of frequency as well as elevation angle. The fluctuations are large for small angles and hence we expect larger error bars in this limit. The error is found to be about 14% for small elevation angles and reduces to about 4% for large angles. The experimental data points are from HiCal2 [9]. The result for the flat surface (section II) is shown for comparison. The only adjustable parameters in our calculation are the parameters in the roughness model and the refractive index. The refractive index has been set equal to the measured value of 1.4. The roughness parameters have been taken to be the same as used in earlier calculations [9]. We see that our theoretical prediction relying on the local plane wave approximation and HiCal-2 data are in good agreement with one another. In more detail, we find that at large elevation angles the calculated values are systematically higher than data but agree within errors. The agreement is found to be better at smaller elevation angles. The computed values depend on the choice of parameters in the roughness model and it is possible to make the

agreement better by adjusting these parameters. However we do not find much motivation to do so since the agreement is already very good with the default parameters being used in the literature.

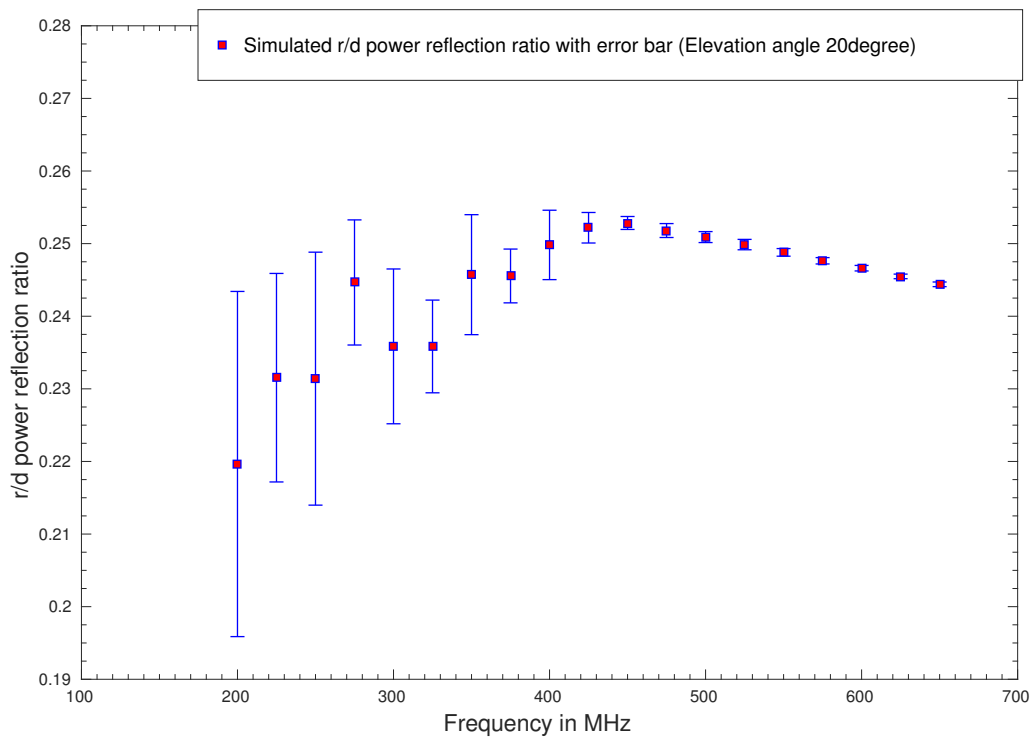


FIG. 4. The ratio of reflected to direct power (r/d) as a function of frequency for $n=1.4$ and elevation angle (angle with respect to ground) of 20 degrees.

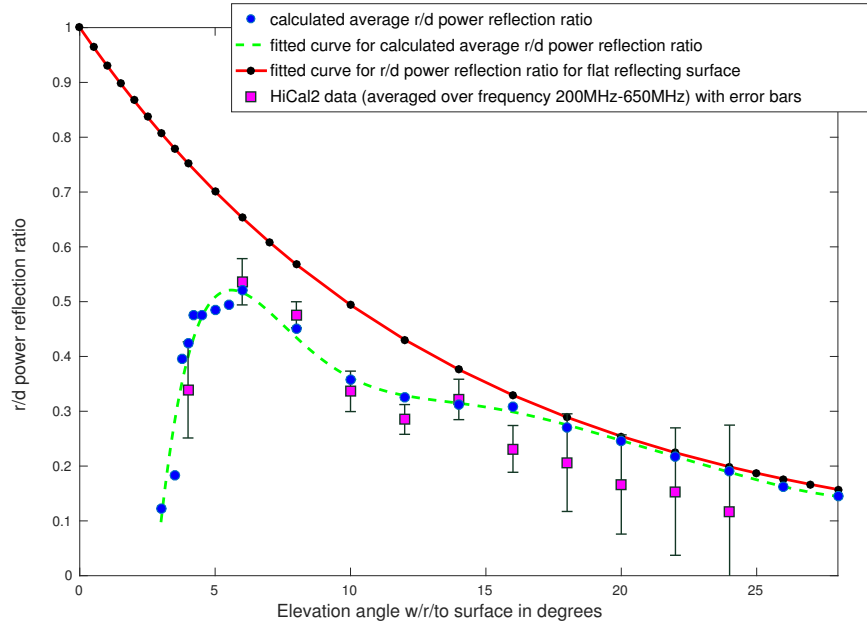


FIG. 5. Comparison of the computed (blue dots) average power reflectance ratio r/d as a function of elevation angle relative to the ground with $n=1.4$ and frequency in the range 200 – 650 MHz with the HiCal-2 experimental results (magenta squares with error bars). The roughness parameters have been chosen to provide a rough match with data without making a detailed fit. The power reflection ratio for a flat surface (without roughness) is shown (red curve and black dots) for comparison. The errors in the theoretical calculation (blue dots) are given in text.

IV. IMPLICATIONS FOR ANITA MYSTERY EVENTS

So far we have considered monochromatic spherical electromagnetic waves and determined their reflection from ice as a function of frequency and the angle of reflection. In the ANITA observations we need to consider electromagnetic pulses. In this section we consider the reflection of such pulses from air-ice interface. We represent each pulse as a superposition of monochromatic spherical waves, which can be treated by the procedure described in earlier sections. The Hertz potential for a monochromatic spherical wave polarized along \hat{y} is given in Eq. 2. The corresponding electric field in the $x - z$ plane in the far zone can be written as

$$\vec{E}_{dir} = k^2 \frac{e^{ikr}}{4\epsilon\pi r} \hat{y} \quad (89)$$

Let $f(p)$ represent the pulse in time domain. The Fourier transform of the pulse can be represented as

$$\tilde{F}(n) = \sum_{p=0}^{N-1} f(p) e^{i \frac{2\pi n p}{N}} \quad (90)$$

where N represents the total number of samples in the time domain. We decompose the Fourier transform into the real and imaginary part

$$\tilde{F}(n) = \tilde{F}_{real}(n) + i \tilde{F}_{imag}(n) \quad (91)$$

The direct electric field at the propagation distance $r = \sqrt{x^2 + y^2 + (z - z_0)^2}$ can be expressed in terms of these by the inverse Fourier transform,

$$\begin{aligned} E_d[p, r] &= \frac{1}{N} \sum_{n=0}^{N-1} [\tilde{F}_{real}[n] + i \tilde{F}_{imag}[n]] \frac{e^{i(kr - \omega(t+t_0))}}{r} \\ &= \frac{1}{Nr} \sum_{n=0}^{N-1} [\tilde{F}_{real}[n] + i \tilde{F}_{imag}[n]] e^{-i \frac{2\pi n p}{N}} \end{aligned} \quad (92)$$

where $\omega = kc$ and we have set $t_0 = kr/\omega$ in order to remove an overall phase. We have also absorbed the overall factor $k^2/4\pi\epsilon$ in Eq. 89 into $\tilde{F}_{real}[n]$ and $\tilde{F}_{imag}[n]$.

For the reflected pulse, we decompose each monochromatic spherical wave using Eq. 1 and determine the corresponding reflected wave. For each plane wave the y -component of the reflected wave is given by Eq. 85. Integrating over all the plane waves, the total reflected field is given by

$$E'_{ref,y} = \int_0^{\frac{\pi}{2} - i\infty} \int_0^{2\pi} \int_{\omega} \frac{ik}{2\pi} \tilde{\Pi}_{S,r} F_{rough}(\omega, \alpha, \beta, \theta_z) \eta(\alpha, \beta, \omega) (\tilde{F}(\omega) e^{-i\omega(t+t_0)}) d\omega d\Omega. \quad (93)$$

where $d\Omega = \sin\alpha d\alpha d\beta$, $\tilde{F}(\omega)$ is the continuous Fourier transform and

$$\eta(\alpha, \beta, \omega) = \left[f_r'^s \cos^2 \tilde{\beta} - f_r'^p \cos \tilde{\alpha} \cos(\tilde{\alpha} - 2\psi) \sin^2 \tilde{\beta} \right], \quad (94)$$

$\tilde{\Pi}_{S,r}$ is given in Eq. 56 and F_{rough} is given in Eq. 86. The final expression for the electric field in terms of the Fourier components (Eq. 91) is given by

$$E_{ref,y}[p] = \frac{1}{N} \sum_{n=0}^{N-1} \frac{k}{2\pi} \left(i \tilde{F}_{real}[n] - \tilde{F}_{imag}[n] \right) e^{-i\omega t} \chi(\omega, \alpha, \beta) \quad (95)$$

$$= \frac{1}{N} \sum_{n=0}^{N-1} \chi(\omega, \alpha, \beta) \frac{k}{2\pi} \left(i \tilde{F}_{real}[n] - \tilde{F}_{imag}[n] \right) e^{-i \frac{2\pi n p}{N}} \quad (96)$$

where

$$\chi(\omega, \alpha, \beta) = \int_0^{\frac{\pi}{2}-i\infty} \int_0^{2\pi} \left[F_{rough} \tilde{\Pi}_{S,r} e^{-i\omega t_0} \left[f_r'^{s} \cos^2 \tilde{\beta} - f_r'^{p} \cos \tilde{\alpha} \cos(\tilde{\alpha} - 2\psi) \sin^2 \tilde{\beta} \right] d\Omega \right] \quad (97)$$

We set $t_0 = (r_1 + r_2)/c$ where r_1 and r_2 are respectively the distances of the source and the detector from the specular point. From this we extract the real part of the final reflected electric field. We clarify that the integral over α receives dominant contributions only from a small region close to the specular point. Hence we do not need to integrate over complex values of α .

In Fig. 6 we show the result for a particular HiCal-1 pulse assuming a reflection angle of 78° using the roughness model given in Eq. 86. As expected we find that the reflected pulse is 180° out of phase with the direct pulse. Although this is to be expected, it is not entirely clear whether it will continue to hold in the presence of surface roughness effects. Hence it is reassuring that the effect emerges in a rigorous formalism without making any uncontrolled approximations and provides further justification for the claim that the ANITA mystery events [3] require Physics beyond the Standard Model [17–21].

Our formalism allows us to examine more complicated roughness models. A detailed investigation along this line is beyond the scope of the present paper. Here we examine how the pulse changes if we make the roughness model asymmetric by setting

$$\rho_\perp^2 \rightarrow x_\perp^2 + \xi^2 y_\perp^2 \quad (98)$$

in Eq. 86. This model essentially leads to different smoothness in different directions. The result for $\xi = 0.25$ is shown in Fig. 7. We find that the main change is the amplitude of the different peaks and dips without any effect on the phase. Hence we find that an asymmetric model of roughness also preserves the phase inversion of the reflected wave. However we do see a significant distortion in the pulse shape with considerable power leaking out from the central pulse. The relative heights of the dominant peak and the dip get inverted as we change ξ from 1 to 0.25. Hence we see that there is some possibility of misidentification of the reflected pulse as a direct pulse even though the phase is not inverted. However if we view the actual pulses observed in ANITA (see Fig. 2 of [22]), we find that the difference in amplitude between the dominant peak and dip is substantial. The roughness effects are relatively small and cannot distort such a pulse to the extent that it can be misidentified. We also try out two other models with the following replacements in Eq. 86: (i) $\vec{\rho}_\perp \rightarrow (\vec{\rho}_\perp - \vec{\rho}_{\perp 0})$;

(ii) $k^2 \rightarrow (k - k_0)^2$ where $\vec{\rho}_{\perp 0}$ and k_0 are constants. The conclusions in both these cases are same as those with model given in Eq. 98. In any case it may be worth investigating this further to see whether we can completely rule out the possibility of such a misidentification. We postpone this to future work.

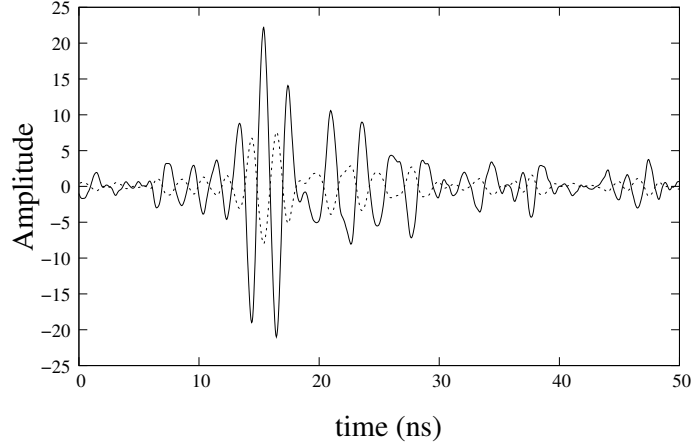


FIG. 6. The direct pulse (solid line) and the reflected pulse (dashed line) using the roughness model given in Eq. 86 and reflection angle of 78°

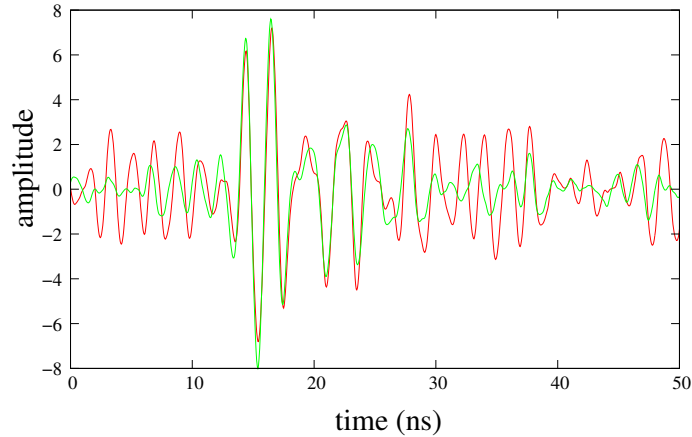


FIG. 7. The reflected pulse for the case of roughness model in Eq. 86 (green line) and the model in Eq. 98 (red line) with reflection angle of 78° .

V. CONCLUSIONS

In this paper we have developed a reliable formalism to handle reflection of spherical electromagnetic wave from a spherical surface. The treatment is based on an expansion of

the spherical wave in terms of plane waves. Each plane wave is reflected from the curved surface by assuming that the reflected wave can be approximated as a plane wave in the neighbourhood of any point. Globally the reflected wave is not a plane wave. The final result is obtained by integrating over all the reflected waves corresponding to different incident plane waves. The procedure involves no uncontrolled approximation. We apply it to ANITA HiCal-2 observations using a reasonable roughness model. We find that our theoretical results for power reflection ratio are in good agreement with data for all the elevation angles observed at HiCal-2. In general we find that our results are close to Fresnel reflection for large elevation angles and, as expected, deviate considerably from Fresnel for small angles. The theoretical calculation also shows rapid oscillations as a function of frequency as well as elevation angle. The fluctuations are found to be rather large for small elevation angles. The final results are obtained after averaging over the frequency range 200-650 MHz relevant for HiCal-2 data. We also apply our procedure in order to determine the reflected pulse profile using as template the pulses generated by HiCal. The main aim of this study is to compare the reflected pulse shape with the incident pulse and to determine if in some cases a reflected pulse can be misidentified as direct. This has application to the observed mystery events by ANITA. We find that the roughness effects can lead to a significant distortion of the signal such that the relative strengths of dominant peak and trough in the reflected wave can get inverted. However the effect is relatively small and can arise only in cases in which these two amplitudes in the direct pulse are not too different. This does not appear to be applicable to the real cosmic ray pulses observed by ANITA. Hence we conclude that roughness effects may not lead to misidentification of ANITA pulses and hence may not provide an explanation for the observed mystery events. However more work is required in order to completely rule out this possibility.

VI. ACKNOWLEDGEMENT

We thank David Besson and Steven Prohira for valuable inputs and discussions throughout this work. We also thank the entire ANITA collaboration for providing us with HiCal-2

reflectivity results and HiCal-1 pulses that we use in this paper.

- [1] P. W. Gorham et al. (ANITA), Phys. Rev. **D82**, 022004 (2010), [Erratum: Phys. Rev. D85, 049901 (2012)], 1003.2961.
- [2] P. Gorham, P. Allison, S. Barwick, J. Beatty, D. Besson, et al., Astroparticle Physics **32**, 10 (2009), ISSN 0927-6505, URL <http://www.sciencedirect.com/science/article/pii/S0927650509000838>.
- [3] P. W. Gorham, J. Nam, A. Romero-Wolf, S. Hoover, et al. (ANITA Collaboration), Phys. Rev. Lett. **117**, 071101 (2016), URL <https://link.aps.org/doi/10.1103/PhysRevLett.117.071101>.
- [4] P. W. Gorham, P. Allison, B. M. Baughman, J. J. Beatty, et al., Phys. Rev. D **85**, 049901 (2012), URL <https://link.aps.org/doi/10.1103/PhysRevD.85.049901>.
- [5] S. Hoover, J. Nam, P. W. Gorham, E. Grashorn, et al., Phys. Rev. Lett. **105**, 151101 (2010), URL <https://link.aps.org/doi/10.1103/PhysRevLett.105.151101>.
- [6] G. A. Askar'yan, Sov. Phys. JETP **14**, 441 (1962), [Zh. Eksp. Teor. Fiz.41,616(1961)].
- [7] G. A. Askaryan, Journal of the Physical Society of Japan Supplement **17**, 257 (1962).
- [8] G. A. Askar'yan, Soviet Journal of Experimental and Theoretical Physics **21**, 658 (1965).
- [9] S. Prohira, A. Novikov, P. Dasgupta, P. Jain, S. Nande, et al. (ANITA Collaboration), Phys. Rev. D **98**, 042004 (2018), URL <https://link.aps.org/doi/10.1103/PhysRevD.98.042004>.
- [10] D. Z. Besson, J. Stockham, et al., Radio Science **50**, 1 (2015).
- [11] P. W. Gorham, P. Allison, et al., Journal of Astronomical Instrumentation **06**, 1740002 (2017).
- [12] H. Schoorlemmer, K. Belov, et al., Astroparticle Physics **77**, 32 (2016), ISSN 0927-6505, URL <http://www.sciencedirect.com/science/article/pii/S0927650516000025>.
- [13] P. W. Gorham, P. Allison, O. Banerjee, L. Batten, J. J. Beatty, K. Belov, D. Z. Besson, et al., ArXiv e-prints (2017), 1710.11175.
- [14] S.-H. Wang (ARIANNA, TAROGE), PoS **ICRC2017**, 358 (2018).
- [15] J. A. Stratton, *Electromagnetic theory*, International series in pure and applied physics (McGraw-Hill, New York, NY, 1941), URL <https://cds.cern.ch/record/105763>.

- [16] A. Romero-Wolf, S. Vance, F. Maiwald, E. Heggy, P. Ries, and K. Liewer, *Icarus* **248**, 463 (2015), ISSN 0019-1035, URL <http://www.sciencedirect.com/science/article/pii/S0019103514006009>.
- [17] J. F. Cherry and I. M. Shoemaker (2018), 1802.01611.
- [18] L. A. Anchordoqui, V. Barger, J. G. Learned, D. Marfatia, and T. J. Weiler, arXiv e-prints arXiv:1803.11554 (2018), 1803.11554.
- [19] G.-y. Huang, *Phys. Rev.* **D98**, 043019 (2018), 1804.05362.
- [20] D. B. Fox, S. Sigurdsson, S. Shandera, P. Mszros, K. Murase, M. Mostaf, and S. Coutu, Submitted to: *Phys. Rev. D* (2018), 1809.09615.
- [21] B. Chauhan and S. Mohanty (2018), 1812.00919.
- [22] P. W. Gorham et al. (ANITA), *Phys. Rev. Lett.* **121**, 161102 (2018), 1803.05088.